

Control of Hybrid Wind-Diesel Standalone Microgrid for Water Treatment System Application

Félix Dubuisson, *Student Member, IEEE*, Miloud Rezkallah, *Member, IEEE*, Ambrish Chandra, *Fellow, IEEE*, Maarouf Saad, *Senior Member, IEEE*, Marco Tremblay, and Hussein Ibrahim

Abstract— This paper deals with the control of a standalone microgrid based on variable speed wind turbine (WT) and fixed speed Diesel Generator (DG) for water treatment application. A Perturb and Observe (P&O) method is used to achieve the Maximum Power Point Tracking (MPPT) from the WT without using speed sensors. Two levels of control are proposed for the three-phase voltage source inverter for voltage and frequency regulation at the Point of Common Coupling (PCC) and power management in standalone and diesel connected modes. Furthermore, the battery energy storage is controlled using simple approach to balance the power in the system during load variations and wind speed changes. The performance of the proposed system is tested using Matlab/Simulink under load and weather variations. In addition, the system is tested on a small-scale prototype in the laboratory under load and wind speed variations.

Index Terms— Diesel generator, perturbation and observation technique (P&O), power management, SRF, standalone microgrid, voltage and frequency regulation, wind turbine

I. INTRODUCTION

MANY facilities, such as water treatment systems are not connected to the main electrical grid. They are powered only from the conventional DG. As known that this energy source is costly and responsible for the emission of greenhouse gases especially when it operates at light loads. Generating electricity locally in these isolated areas from Renewable Energy Sources (RES), such as wind or solar is a good way to answer these drawbacks [1]. However, combination of RES with the existing DG is a complex process; it requires advanced control and additional reliable

elements such as energy storage system to compensate their intermittency [2]. Moreover, complex control strategies are needed to ensure a stable operation and clean uninterruptible power supply to the water treatment station as application, which is considered as a critical load.

According to [3], the most of isolated microgrids are operating using a droop control strategy. This control technique can regulate the voltage and frequency as well as achieve power sharing. Droop control possesses different advantages such as simplicity, robustness and ability to operate without resorting to communication between system elements [4]. However, each energy source is independent and adapt its voltage and frequency references based on the powers measured at the PCC. Usually, the frequency reference is regulated with controlling the active power variations and the voltage references are regulated by controlling the reactive power variations, that is why this control technique is identified as P-f and Q-V droop. It is reported in [5], that droop control is not perfect and possesses drawbacks, such as the high droop coefficients, which can compromise the grid stability, by the deviations in voltage and frequency. In addition, its implementation is hard due to the complex transformation needed. Many, droop-based control strategies are proposed in the literature to compensate these drawbacks [6-7]. In [6], an adaptive voltage droop control, is proposed to tune the voltage droop coefficients, to compensate the mismatch of the different energy sources voltage output, and to improve the reactive power sharing. For this technique, communication is suggested to achieve high performances from the adaptive voltage droop strategy and if the communication system is interrupted the controller operates using last tuned droop coefficients. This control technique is more efficient than conventional droop control system where the obtained experimental results show that the reactive power sharing is done properly, and that the system is not affected by delay time caused by communication system. In [7], droop-based strategy to control the inverter in a microgrid, is proposed. This control technique is validated in simulation using Matlab Simulink and in real time through hardware prototype. The obtained results under different conditions show satisfactory performances in terms of power sharing and voltage as well as frequency regulation at the PCC.

In the same context, authors in [8] proposed Synchronous

F. Dubuisson, M. Rezkallah, A. Chandra and M. Saad are with the Department of Electrical Engineering, École de Technologie Supérieure, Montreal, QC H3C 1K3, Canada (e-mail: felix.dubuisson.1@ens.etsmtl.ca, cc-miloud.rezkallah@etsmtl.ca; ambrish.chandra@etsmtl.ca, maarouf.saad@etsmtl.ca).

M. Tremblay is with the SUEZ Treatment Solutions, Montréal, QC H4R 2K9, Canada (e-mail: Marco.Tremblay@suez-na.com)

M. Rezkallah and H. Ibrahim is with the Cégep de Sept-Îles, Sept-Îles, QC G4R 5B7, Canada (e-mail: miloud.rezkallah@itmi.ca Hussein.Ibrahim@cegepsi.ca).

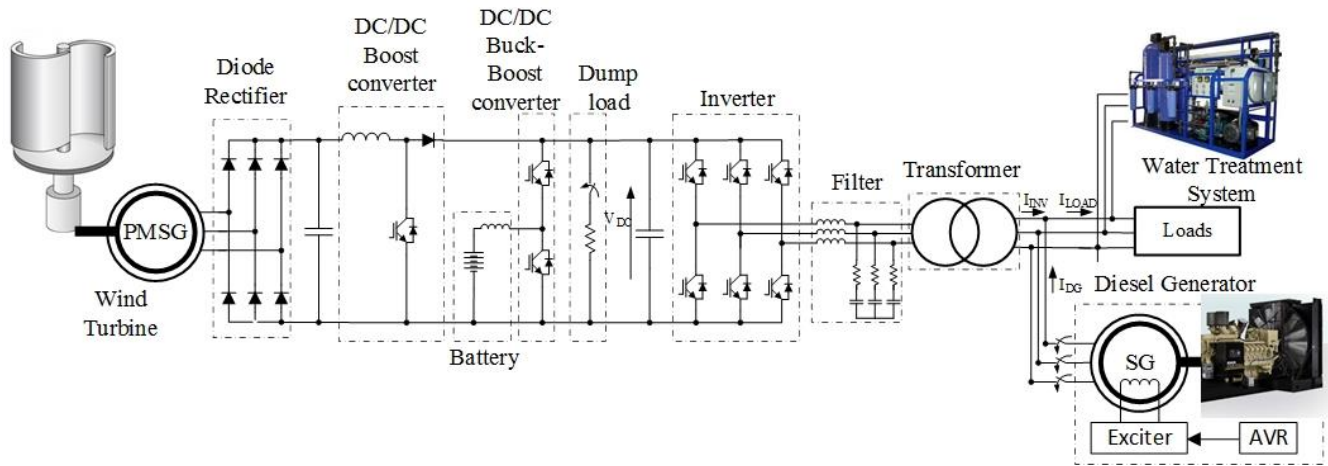


Fig. 1. Configuration of the proposed standalone microgrid

Reference Frame (SRF) control. This technique is a well-developed technique for three-phase converters control. It controls the current and guarantees a good dynamic performance, as well as zero steady-state error during transitions. The measured current is transformed from the stationary frame into the rotating frame and can be regulated using PI controllers. This control technique is used to control Active Power Filter (APF) and Unified Power Quality Conditioner (UPQC) as detailed in [9]. Unfortunately, it requires decisive PLL techniques. However, in grid connected systems, the voltage and frequency are considered as constant, so, synchronization with PCC is not a big issue but in standalone systems where the DG operates only when needed, a robust technique for the synchronization between the inverter and the PCC, is needed.

UPQCs are controlled to manage the power in hybrid microgrids and improve the power quality [9]. They are composed of two back-to-back inverters sharing a DC link. The first inverter is controlled as a voltage source and the second as an active filter. Consequently, one ensures the voltage regulation at the PCC and delivers power to compensate load variations while the other one improves power quality. Unfortunately, the use of two back-to-back inverters increase the number of power converters, which leads to an increase the hardware complexity, consequently its cost is increasing as well. In [10], authors proposed a droop-based control strategy controlling UPQC to ensure a proper power flow between the AC and the DC side. The obtained results show good performances under severe conditions, such as nonlinear load and the reactive power sharing is done properly, as well as, the AC voltage regulation at the PCC. In [11], a new SRF based control is proposed for UPQC with an improved PLL. This method is simpler and easier to implement, as it needs reduced number of current sensors. In addition, the reactive power and harmonic compensation are done properly under presence of unbalanced linear and non-linear loads.

Wind Energy Conversion System (WECS) based on Permanent Magnet Synchronous Generator (PMSG) has gained more and more interests in microgrid applications. WT

based PMSG possesses various advantages such as no need of electrical excitation, higher efficiency, higher number of poles, higher power density, also they are easier to control and no needs gearbox [12] [13]. Moreover, this technology usually requires power converters to achieve stable operation with high efficiency. To achieve high efficiency from WT driven variable speed PMSG, Maximum Power Point Tracking (MPPT) based control, is required. Many MPPT techniques are proposed in the literature [14-17], such as Tip-Speed Ratio (TSR) technique, Optimum Relation Based (ORB) technique, and Perturbation and observation (P&O) technique.

According, to [15], these MPPT methods possess advantages and drawbacks, which should be solved. Among these drawbacks, there is the necessity of mechanical sensors. Presence of this sensors lead to increase of the cost and hardware complexity of installation [16]. Generally, P&O method require only output voltage and current of the WT. according to [16], it is so hard to find a good step size which ensures a fast convergence of the control when system is subjected to the sudden wind variations without any oscillation around the MPP. In [17], a P&O technique based on integral action, is proposed. A correlation between the variations of the power and the voltage at the input of the DC-DC boost converter is used, therefore only electrical measures are needed.

In [18], control of wind-diesel hybrid system for standalone application to reduce the fuel consumption, is proposed, and in [19], battery storage system is employed to achieve high performances and reduce the fuel consumption in standalone microgrid. In [18,19], DG is kept running at all time, which is not effective, costly and can affect the lifespan of the DG.

To solve these issues and achieve high performances in standalone microgrid for water treatment applications, the following solutions, which represent the contributions of this research work, are proposed,

1) Design of a new and simple standalone micro-grid configuration based on fixed speed DG and WT driven variable speed PMSG for water treatment station without any mechanical sensors.

2) Enhanced power sharing strategy to regulate the voltage and frequency at the PCC.

3) Less fuel consumption by reducing the time running of DG and maximizing its efficiency by operating the DG only at its rated power.

4) Robust and simple control strategy for the DC-DC buck-boost converter to ease the bidirectional power flow through the battery.

5) Enhanced MPPT technique, which is proposed first in [17].

6) Validation in real time of all proposed concept for water treatment system application.

This paper is organized as follows, in section II the proposed standalone microgrid is presented with its operation mode. In section III, all developed control strategies are detailed. In section IV, simulation and experimental results as well as discussion are given, and the conclusion is presented in Section V.

II. STANDALONE MICROGRID CONFIGURATION

Fig. 1 shows the proposed standalone microgrid configuration. It consists of Diesel Engine (DE) driven fixed speed Synchronous Generator (SG) and WT driven variable speed Permanent Magnetic Synchronous Generator (PMSG), which is connected to the common DC bus through a diode rectifier and controlled DC-DC boost converter. A battery pack of Nickel Cadmium technology is used to balance the power in the system. To protect the battery from overcharging a DC dump load, is employed. For a galvanic isolation between the AC and the DC bus, a delta-star transformer is employed. The water treatment system is considered as a load and is connected to the AC bus.

In Table 1, different operation modes of the system shown in Fig. 1, are detailed. The operation mode depends on the state of charge (SOC) of the battery, the power generated by the WT (P_{WT}) and the power consumed by the load (P_{LOAD}). For each mode, the energy sources are detailed, as well as, the SOC of the battery.

The DG is used as a backup energy source, it starts only when the SOC of the battery gets lower than 50% and stop when the SOC reaches 70%. The DG charges the battery and supply the load at the same time. The battery charges much faster if the WT is delivering power at the same time, but the DG can supply the load and charges the battery on its own.

TABLE I
SYSTEM OPERATION MODES

Mode	Conditions	Energy sources	State of the battery
Mode 1	$P_{WT} > P_{LOAD}$ SOC > 50%	WT	Charging
Mode 2	$P_{WT} < P_{LOAD}$ SOC > 50%	WT + Battery	Discharging
Mode 3	$P_{WT} < P_{LOAD}$ SOC < 50%	DG	Charging
Mode 4	$P_{WT} > P_{LOAD}$ SOC < 50%	DG + WT	Fast charging
Mode 5	$P_{WT} > P_{LOAD}$ SOC > 70%	WT	Charging
Mode 6	$P_{WT} > P_{LOAD}$ SOC = 100%	WT + Battery	Discharging in the Dump Load

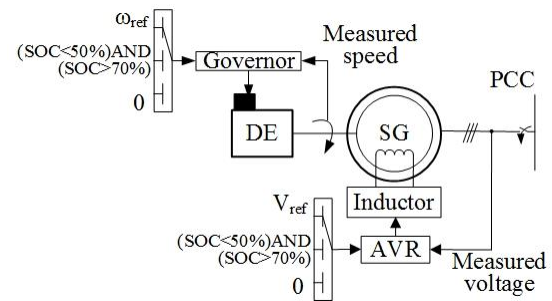


Fig. 2. Control strategy for the DG

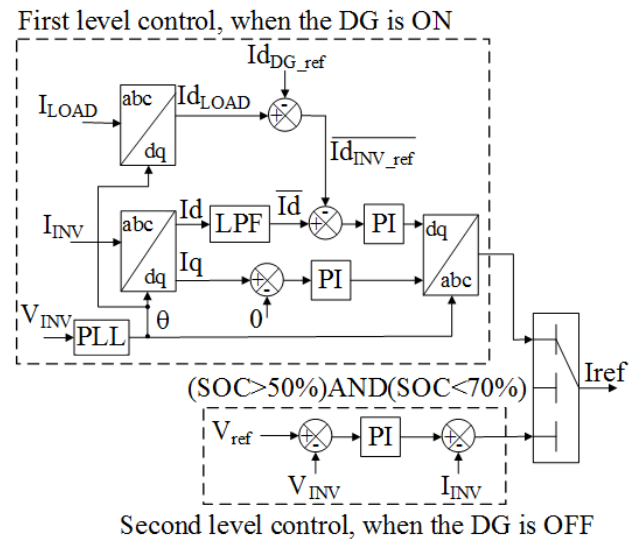


Fig. 3. Two-level control strategy for the three-phase inverter

III. CONTROL SYSTEM

In this section, the developed control strategies of the different elements of the system, are detailed.

A. Control strategy for the DG

Regarding the control strategy of the DG, it can be seen on Fig. 2. A governor compares the measured speed with its reference and the error is fed to Proportional Integral (PI) controller that decide the amount of fuel required to increase or decrease the speed of the engine in order to regulate the frequency at the PCC. The Automatic Voltage Regulation (AVR) compares the voltage measured at the PCC with its reference and the error is fed to a PI controller to obtain the field voltage required to generate the excitation current for SG.

B. Control Strategy for the Three-Phase Inverter

The developed control strategy for the three-phase inverter is illustrated in Fig. 3. It consists of two-level control. When the DG is turned on, the inverter is responsible for balancing the powers between the AC and the DC side of the microgrid and the first level control, is used. The inverter current is converted from the stationary frame to the rotating frame using Park transformation.

$$\begin{bmatrix} i_d \\ i_q \\ i_o \end{bmatrix} = \frac{2}{3} \begin{bmatrix} \sin \theta & \sin\left(\theta - \frac{2\pi}{3}\right) & \sin\left(\theta + \frac{2\pi}{3}\right) \\ \cos \theta & \cos\left(\theta - \frac{2\pi}{3}\right) & \cos\left(\theta + \frac{2\pi}{3}\right) \\ \frac{1}{2} & \frac{1}{2} & \frac{1}{2} \end{bmatrix} \begin{bmatrix} i_a \\ i_b \\ i_c \end{bmatrix} \quad (1)$$

The inverter direct current reference (I_{dINV_ref}) is calculated using the sensed load current (I_{dLOAD}) and the DG current reference (I_{dDG_ref}). Using the DG current reference makes sure that the DG operates at its rated power. A PI controller is used to compare the sensed direct inverter current to this new reference. Regarding the q component of the inverter current, it is forced to zero thanks to a PI controller to minimize the reactive power exchanges between the AC and the DC side of the microgrid. The inverter current reference in the rotating frame is fed to a hysteresis controller in order to create the signal switches of the inverter as,

$$\begin{cases} I_{dref} = \left(k_{pd} + \frac{k_{id}}{s}\right) (\bar{I}_d - (I_{dLOAD} - I_{dDG_ref})) \\ I_{qref} = \left(k_{pq} + \frac{k_{iq}}{s}\right) (I_q - 0) \end{cases} \quad (2)$$

A PLL is needed to obtain the phase shift (θ) for the transformations between the rotating and the stationary frames. The phase shift (θ) is calculated using in-phase and quadrature unit templates, which are calculated as follows,

$$\begin{cases} u_{ap} = \frac{v_{La}}{V_L} \\ u_{bp} = \frac{v_{Lb}}{V_L} \\ u_{cp} = \frac{v_{Lc}}{V_L} \end{cases} \quad (3)$$

Where v_{La} , v_{Lb} and v_{Lc} are the line to line voltage and V_L is the amplitude of the AC voltage. The quadrature units are calculated as follows:

$$\begin{cases} u_{aq} = \frac{1}{\sqrt{3}} (-u_{bp} + u_{cp}) \\ u_{bq} = \left(\frac{\sqrt{3}}{2} u_{ap} + \frac{1}{2\sqrt{3}} (u_{bp} - u_{cp})\right) \\ u_{cq} = \left(-\frac{\sqrt{3}}{2} u_{ap} + \frac{1}{2\sqrt{3}} (u_{bp} - u_{cp})\right) \end{cases} \quad (4)$$

The frequency is obtained based on the following equations as,

$$\omega_s = \cos \theta \frac{d}{dt} (\sin \theta) - \sin \theta \frac{d}{dt} (\cos \theta) \quad (5)$$

$$\begin{cases} \cos \theta = u_{aq} \\ \sin \theta = u_{ad} \end{cases} \quad (6)$$

If the DG is turned off, the inverter supplies the connected loads and ensures regulation of the frequency as well as the voltage at the PCC. These tasks are achieved by selecting the

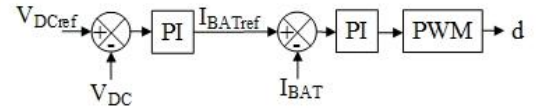


Fig. 4. Control strategy for the DC-DC Buck-boost Converter

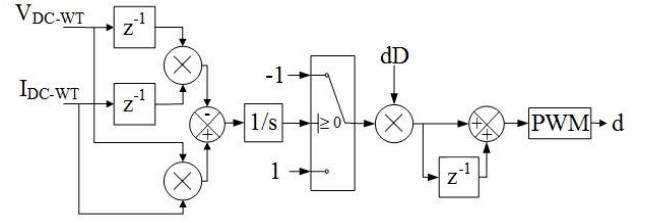


Fig. 5. MPPT strategy for the WT

second level control. The measured voltage at the PCC is compared with its reference and the error is fed to PI controller and the current measured at the PCC is subtracted from the output of the PI controller in order to get the new current references as,

$$I_{INV_ref} = \left(\left(k_p + \frac{k_i}{s}\right) (V_{ref} - V_{INV})\right) - I_{INV} \quad (7)$$

C. Control Strategy for the DC-DC Buck-Boost Converter

Fig. 4 shows the control strategy for the DC-DC buck-boost converter. A PI controller is used to regulate the DC link voltage. The output of the PI controller represents the battery current reference and is compared with the sensed battery current and the output of the PI controller is the control signal which is fed to PWM to get the switches signals of the buck-boost converter.

$$I_{BATref} = \left(k_{p1} + \frac{k_{i1}}{s}\right) (V_{DCref} - V_{DC}) \quad (8)$$

$$d = \left(k_{p2} + \frac{k_{i2}}{s}\right) (I_{BATref} - I_{BAT}) \quad (9)$$

D. MPPT Approach for the WECS

The control strategy used to achieve MPPT from the WT is shown in Fig. 5. As already mentioned, the proposed control technique for MPPT from WT does not need speed sensor, only output voltage and current are used to compute the power at n^{th} and $(n-1)^{th}$ instants as,

$$P_{WT}(n) = V_{WT}(n) i_{WT}(n) \quad (10)$$

$$P_{WT}(n-1) = V_{WT}(n-1) i_{WT}(n-1) \quad (11)$$

The sign of the power variation is used to determine the sign of the incremental step to reach the MPP.

$$\begin{cases} k=1 \text{ if } (P_{WT}(n) - P_{WT}(n-1)) > 0 \\ k=-1 \text{ if } (P_{WT}(n) - P_{WT}(n-1)) < 0 \end{cases} \quad (12)$$

As detailed in Fig. 5, dD is the incremental step, it is responsible for the speed of convergence but also for the size

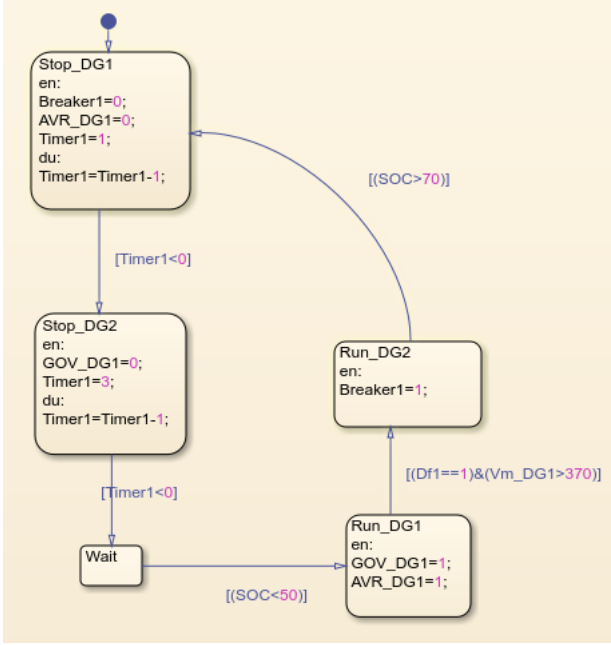


Fig. 6. State flow chart to control AVR, governor and the controlled switch

of the oscillations. According to [20], the step size dD should be 0.5% in order to get a good compromise between speed of convergence to the MPP and oscillations around the MPP.

E. Control Strategy for the Dump- Load

The dump load is used to protect the battery from overcharging. Its switch is turned off only if the SOC of the battery is fully charged.

F. Power Flow Supervisor

A supervisor based on state flow chart is used to turn ON and OFF the DG. As one can see on Fig. 6, the DG is turned ON only based on the SOC of the battery. Once the SOC of battery becomes less than 50%, the governor and AVR are turned ON and once the system frequency and the terminal stator voltage of the DG are equal to the system frequency and the AC voltage at the PCC, the controlled switch is turned on. If the SOC of the battery is high or equal to 70%, the controlled switch, AVR and governors, are turned off.

G. Optimal method for PI gain tuning

The PI controller have two parameters: k_p and k_i to tune. The following technique, which is based on determination of the transfer function of the control loop, is applied to get the optimal gains of the proposed PI controllers. As is detailed in Fig. 7 and 8, the transfer function in open loop of the DC-voltage control loop is described as:

$$G_v(s) = \frac{U_{DC}}{\tilde{V}_{DC}} = k_p \frac{s + \frac{k_i}{k_p}}{s} \quad (13)$$

And the closed loop is given as:

$$\frac{V_{DC}}{V_{DC}^*} = 2\zeta\omega \frac{s + \frac{\omega}{2\zeta}}{s^2 + 2\zeta\omega s + \omega^2} = \frac{k_p s + k_i}{s^2 + \frac{k_p}{C_{DC}} s + \frac{k_i}{C_{DC}}} \quad (14)$$

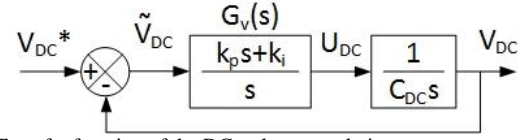


Fig. 7. Transfer function of the DC-voltage regulation

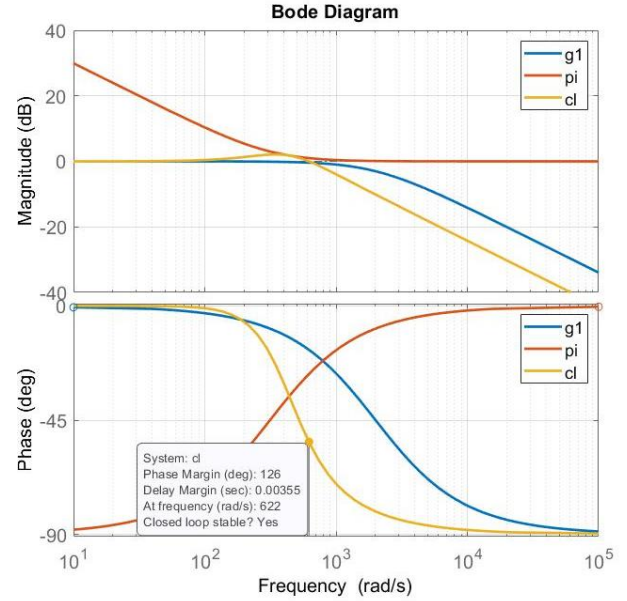


Fig. 8. Bode diagrams of the transfer function, PI controller and closed loop system.

Based on (14), one obtains the gains as:

$$k_p = 2\zeta\omega C_{DC} \quad (15)$$

$$k_i = \omega^2 C_{DC} \quad (16)$$

Selecting, ζ and ω equal to 0.7 and 439.82 rad/s as detailed in [21], one obtains a good compromise between the static and dynamic performances.

The C_{DC} is selected equal to =500e-6F. The optimal gains that ensure less overrun and fast response time as presented in Fig.8 are selected as, $k_p=0.3079$ and $k_i=96.7208$.

IV. SIMULATION AND EXPERIMENTAL RESULTS

To validate the different control approaches presented above and test the performances of the proposed standalone microgrid, many scenarios are tested and validated using simulations on Matlab/Simulink and in real time through small-scale hardware prototype of 2 kW.

A. Simulation Results under Load and Wind variations

Fig. 9 shows the waveforms of the PCC voltage and its magnitude, the load current, DG current, inverter current, battery current, WT current, voltage of the DC bus, SOC of the battery, and system frequency. During this test, the wind varies as follows: it starts at $t=7s$ and increases until $t=8s$, then it stays constant until $t=11s$, next it starts decreasing until $t=15s$ and stays constant until $t=16s$, where it increases until $t=18s$ and then it stays constant until the end of the simulation. The load is varying between $t=7s$ and $t=9s$ and at $t=18s$.

One can see that the WT current varies with the wind speed variations and that the PCC voltage and frequency are well regulated at their rated values, which are 460V and 60 Hz. The DC voltage oscillates during wind and load variations, but it is regulated around its rated value, which is equal to 350V. In addition, one can see that the battery is charging very slowly from $t=2s$ to $t=7s$, this is due to the absence of wind. Then, from $t=7s$ to $t=10.7s$, it starts charging much faster when the DG and the WT are providing power. At $t=10.7s$, the SOC of the battery is equal to 70% so the DG is turned off. Between $t=10.7s$ and $t=18s$, the WT is not delivering enough power to supply the load, so the battery is discharging to help the wind turbine supply the load. At $t=18s$, the load is reduced, and the WT is delivering enough power to supply the load and charge the battery at the same time. Therefore, one can say that both the DG and the WT can charge the battery and supply the load simultaneously. Which leads to say that the battery is helping the system to maintain its stability by balancing the powers.

On Fig. 10 one can see the active and reactive power of the

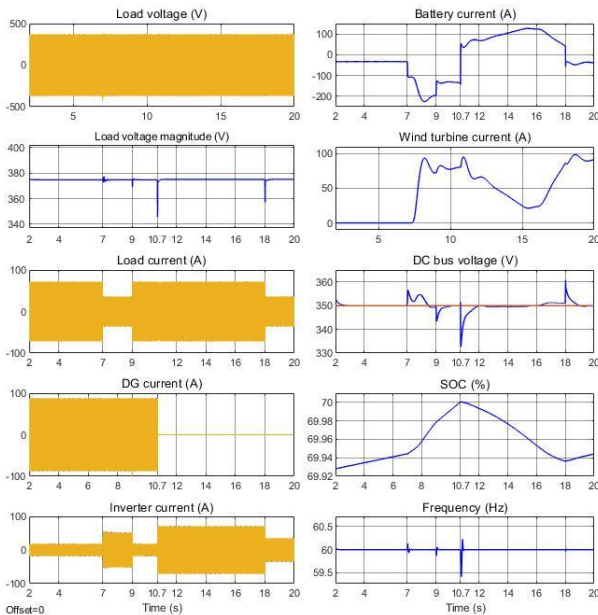


Fig. 9. Simulation results under load and wind variations

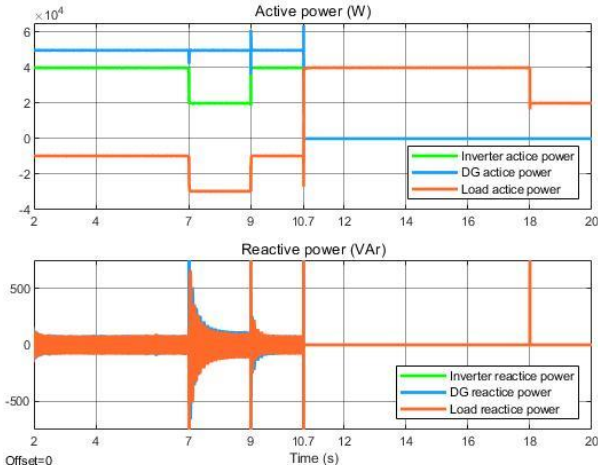


Fig. 10. Active and reactive power of the system under weathered and load variations.

load, the DG and the inverter. One can see the exchange of active power between $t=2s$ and $t=10.7s$, when the DG is charging the battery. Also, one can see that the DG is always producing the same amount of power, which is its rated power. And when the DG is off, the inverter is supplying the load on its own. Regarding reactive power one can see a small exchange of reactive power between the DG and the inverter. These exchanges can reach 500 Var when the load is varying but they are about 100 Var in steady state, so one can consider they are insignificant.

To validate the performances of the dump-load another test was done. Fig. 11 shows the waveforms of the PCC voltage and its magnitude, the load current, dump load current, inverter current, battery current, WT current, voltage of the DC bus, SOC of the battery, and the system frequency. As one can see, at $t=6.65s$ the SOC of the battery reaches 100% and the dump load is activated to dissipate the power and protect

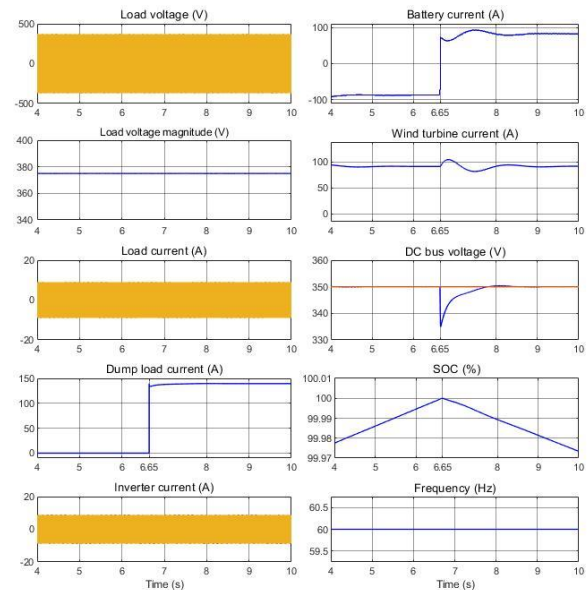


Fig. 11. Simulation results of the dump load system

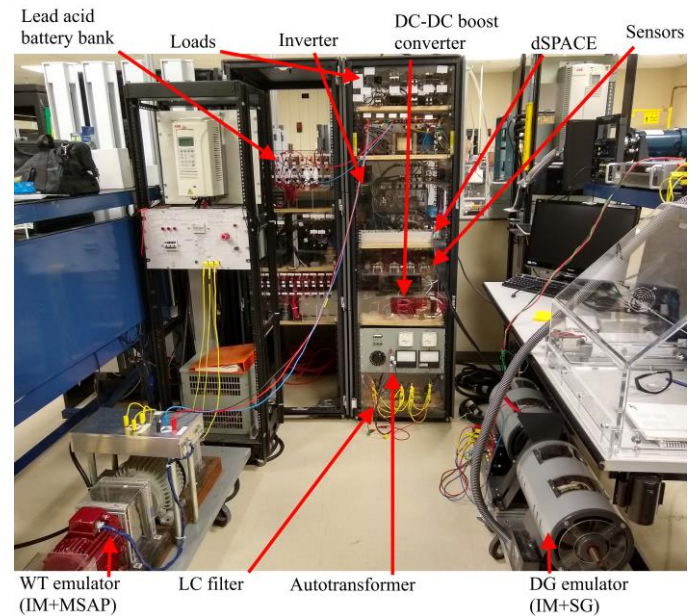


Fig. 12. Hardware configuration

the battery from overcharging. One can see that the load voltage, frequency and DC bus voltage are well regulated. This confirms that battery is protected from overvoltage and system is able to operate in this operation mode without any unbalance or frequency deviation.

B. Experimental Results Under Load and Wind Variations

Fig. 12 shows the hardware configuration used to validate the results obtained with the simulation. It is composed of DG (Induction Motor (IM) driven SG), synchronization switch, inverter, boost converter, variable voltage transformer, LC filter, dSPACE controller, lead acid batteries, WT (IM driven PMSG), and loads.

Fig. 13 demonstrates the performances of the Diesel-Battery system under load variations. In Fig. 13 (a) and (b), the

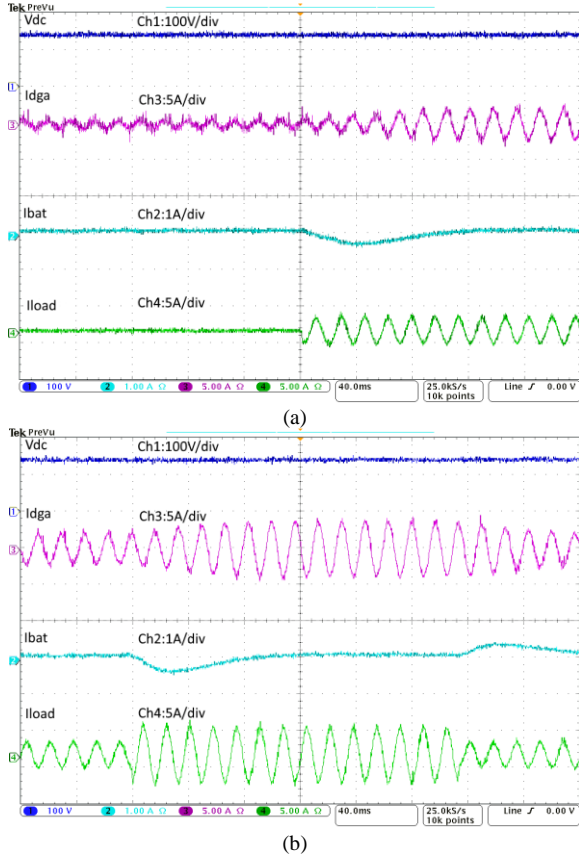


Fig. 13. Dynamic performances of the Diesel-Battery system under load variations

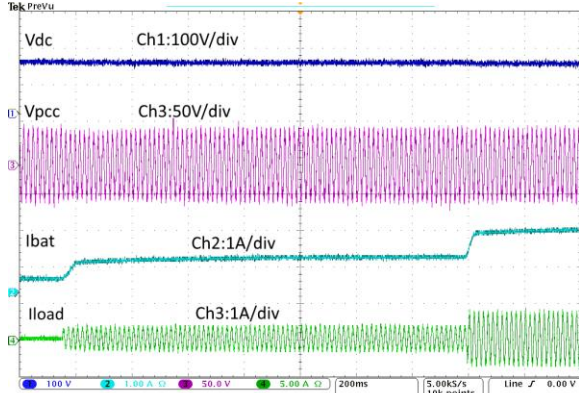


Fig. 14. Dynamic performances of the Battery system without Diesel under load variations

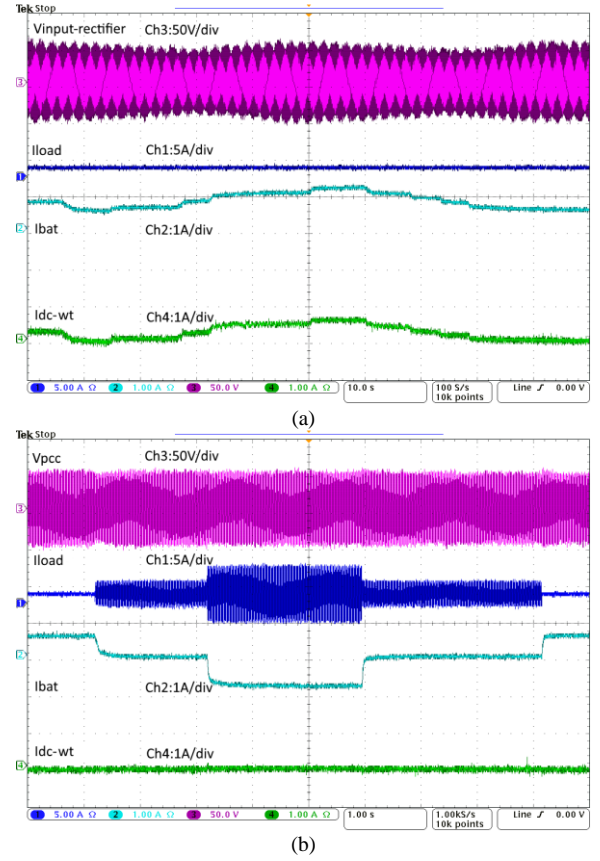


Fig. 15. Dynamic performances of the Battery-WT system under load and wind speed variations

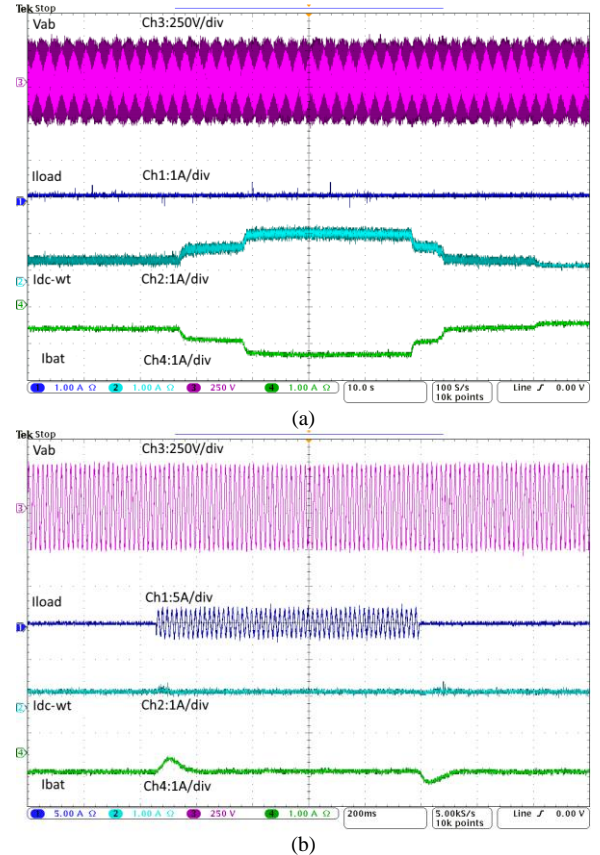


Fig. 16. Dynamic performances of the Diesel-Battery-WT system under load and wind speed variations

waveforms of the DC bus voltage, DG current, battery current and load current are shown. One can see that the DG is producing current even when there is no load and that the current charges the battery. Also, one can see that the dynamic of the DG is slow when the load increases and that the battery delivers or absorb more current during the load variations. So, one can say that the battery helps to keep stable the operation by balancing the powers in the system. One can clearly see that the DC voltage is well regulated in this operation mode, which confirms the robustness of the developed control strategy for the DC-DC buck boost converter.

In Fig. 14, the waveforms of the DC bus voltage, the voltage of the PCC, the battery current and the load current are shown. One can see that the battery can provide power to the load at any time. It is observed that during absence of load, the battery is discharging slowly, this is due to the passive elements of the system. In this operation mode, the DC voltage is well regulated, which confirms the robustness of the developed control strategy for the DC-DC buck boost converter.

In Fig. 15 (a) the voltage measured after the MSAP, the load current, the battery current and the DC current measured after the DC-DC boost converter, are presented. In this test, there is no load and the wind speed are varying. One can see that the battery is being charged by the WT. In Fig. 15 (b) the waveforms of the voltage at the PCC, the load current, the battery current and the DC current measured after the DC-DC boost converter, are shown. In this test, the wind speed is kept constant, and load varies. One can see that when load is removed, WT charges the battery. When load increase at $t=1.2s$, the battery stops charging because the current produced by the WT is used to supply the connected load. When load is increased more at $t=3.2s$, battery is discharging in order to balance the power in the system. Then one can observe the same phenomena when the load is decreasing. Once again, the battery helps the system to remain stable.

In Fig. 16, the waveforms of the DG voltage, the load current, the DC current of the WT and the battery current, are shown. To test the performance of the proposed configuration as well as the developed control algorithms, two testes are performed. In Fig. 16 (a), load is completely removed, and the wind speed varies with time. It is observed that DG and the WT charge the battery. In Fig. 16 (b), the wind speed is considered constant and the load varies with time. One can observe that the battery balance power in the system when load is increased. These experimental tests show the same results obtained with the simulations. Both the DG and the WT can charge the battery and supply the load simultaneously. It is observed that the battery contributes to maintain the stability of the system by balancing the powers in each operation mode.

V. CONCLUSION

In this paper, a standalone microgrid for small water station is designed and validated using simulations with Matlab/Simulink and experimental tests on a small-scale prototype. An improved control strategy based on SRF was

developed to operate the DG efficiently at its rated power by controlling the three-phase voltage source inverter. The obtained results in the presence of severe conditions show satisfactory performance without any saturation of the controllers and with less overrun and fast response time. The voltage and frequency regulation at the PCC as well as power sharing, are achieved at different operation modes and during transitions. It has been demonstrated that the DG was used as back up energy sources and that the load is supplied at all time with a stable power without any interruption.

APPENDIX

TABLE II
SYSTEM PARAMETERS

Elements	Parameters and Values
WECS	$P=50kW$, $V_{dc}=288V$, $\omega=12500$ rpm, $R_s=0.0041 \Omega$, $L_d=8.7079e-05H$, $L_q=1.4634e-04H$, Flux linkage= $0.07V.s$, $J=0.089kg.m^2$, $F=0.005N.Més$, $T_f=4N.m$
Battery	nominal voltage= $250V$, cut-off voltage= $187.5V$, fully charge voltage= $286V$, energy capacity= $100KWh$, nominal discharge current= $80A$, internal resistance= 0.00625Ω
SG	$S_n=52.5kVA$, $V_n=460V$, $f_s=60Hz$, $2P=4$, $R_s=0.0181\Omega$, $L_l=0.0009622H$, $L_{mq}=0.02683H$, $L_{mq}=0.01187H$, $J=0.3987kg.m^2$, $F=0.031N.m.s$
AC bus	$V_{LLrms}=460V$, Frequency= $60Hz$
Load	Maximum load= $40kW$

TABLE III
SMALL SCALE PROTOTYPE PARAMETERS

Elements	Parameters and Values
DG	$P=2kW$, $\omega=1800rpm$, $V=208$, $I=6.8A$, $f_s=60Hz$,
Battery	$V=120V$
WECS	$P=2.5kW$, $\omega=1800$ rpm, $V=280V$, $I=5.1A$
AC bus	$V_{LLrms}=40V$, Frequency= $60Hz$
Load	$40kW$

REFERENCES

- [1] Y. Han, P. Shen, X. Zhao, and J. M. Guerrero, "Control strategies for islanded microgrid using enhanced hierarchical control structure with multiple current-loop damping schemes," *IEEE Transactions on Smart Grid*, vol. 8, no. 3, pp. 1139-1153, May 2017.
- [2] Y. Karimi, H. Oraee, M. S. Golsorkhi, and J. M. Guerrero, "Decentralized Method for Load Sharing and Power Management in a PV/Battery Hybrid Source Islanded Microgrid," *IEEE Transactions on Power Electronics*, vol. 32, no. 5, pp. 3525-3535, May 2017.
- [3] S. K. Sahoo, A. Sinha, and N. Kishore, "Control Techniques in AC, DC, and Hybrid AC-DC Microgrid: A Review," *IEEE Journal of Emerging and Selected Topics in Power Electronics*, vol. 6, no. 2, pp. 738-759, June 2018.
- [4] Y. Sun, X. Hou, J. Yang, H. Han, M. Su, and J. M. Guerrero, "New perspectives on droop control in AC microgrid," *IEEE Transactions on Industrial Electronics*, vol. 64, no. 7, pp. 5741-5745, July 2017.
- [5] A. Micalef, M. Apap, C. Spiteri-Staines, J. M. Guerrero, and J. C. Vasquez, "Reactive power sharing and voltage harmonic distortion compensation of droop controlled single phase islanded microgrids," *IEEE Transactions on Smart Grid*, vol. 5, no. 3, pp. 1149-1158, May 2014.
- [6] Mahmood, Hisham, Dennis Michaelson et Jin Jiang. 2015. "Reactive power sharing in islanded microgrids using adaptive voltage droop control," *IEEE Transactions on Smart Grid*, vol. 6, no 6, p. 3052-3060, Nov. 2015.
- [7] Dubuisson, F, M Rezkallah, A Chandra, M Saad et M Tremblay. 2018. "Implementation of a new control for hybrid wind-diesel for water treatment standalone system," In 2018 *IEEE Industry Applications Society Annual Meeting (IAS)*, p. 1-5. IEEE.

- [8] Han, Yang, Hao Chen, Zipeng Li, Ping Yang, Lin Xu et Josep M Guerrero. 2019. "Stability Analysis for the Grid-Connected Single-Phase Asymmetrical Cascaded Multilevel Inverter With SRF-PI Current Control Under Weak Grid Conditions," *IEEE Transactions on Power Electronics*, vol. 34, no 3, p. 2052-2069, March 2019.
- [9] Kesler, Metin, et Engin Ozdemir. 2011. "Synchronous-reference-frame-based control method for UPQC under unbalanced and distorted load conditions," *IEEE Transactions on Industrial Electronics*, vol. 58, no 9, p. 3967-3975, Sept. 2011.
- [10] P. G. Khorasani, M. Joorabian, and S. G. Seifossadat, "Smart grid realization with introducing unified power quality conditioner integrated with DC microgrid," *Electric Power Systems Research*, vol. 151, pp. 68-85, Oct. 2017.
- [11] Kesler, Metin, et Engin Ozdemir. 2011. "Synchronous-reference-frame-based control method for UPQC under unbalanced and distorted load conditions," *IEEE Transactions on Industrial Electronics*, vol. 58, no 9, p. 3967-3975, Sept. 2011.
- [12] L. Trilla, F. D. Bianchi, and O. Gomis-Bellmunt, "Linear parameter-varying control of permanent magnet synchronous generators for wind power systems," *IET Power Electronics*, vol. 7, no. 3, pp. 692-704, March 2014.
- [13] R. Engleitner, A. Nied, M. S. M. Cavalca, and J. P. da Costa, "Dynamic Analysis of Small Wind Turbines Frequency Support Capability in a Low-Power Wind-Diesel Microgrid," *IEEE Transactions on Industry Applications*, vol. 54, no. 1, pp. 102-111, Feb. 2018.
- [14] Z. M. Dalala, Z. U. Zahid, W. Yu, Y. Cho, and J.-S. J. Lai, "Design and analysis of an MPPT technique for small-scale wind energy conversion systems," *IEEE Transactions on Energy Conversion*, vol. 28, no. 3, pp. 756-767, Sept. 2013.
- [15] J. Chen, T. Lin, C. Wen, and Y. Song, "Design of a unified power controller for variable-speed fixed-pitch wind energy conversion system," *IEEE Transactions on Industrial Electronics*, vol. 63, no. 8, pp. 4899-4908, Aug. 2016.
- [16] Y. Zhao, C. Wei, Z. Zhang, and W. Qiao, "A review on position/speed sensorless control for permanent-magnet synchronous machine-based wind energy conversion systems," *IEEE Journal of Emerging and Selected Topics in Power Electronics*, vol. 1, no. 4, pp. 203-216, Dec. 2013.
- [17] H. Abouobaida, "New MPPT control for wind conversion system based PMSG and a comparison to conventional approaches," in *Systems, Signals & Devices (SSD)*, 2017 14th International Multi-Conference on, 2017, pp. 38-43: IEEE.
- [18] Tiwari, Shailendra Kr, Bhim Singh, and Puneet K. Goel. "Control of Wind-Diesel Hybrid System with BESS for Optimal Operation," *IEEE Transactions on Industry Applications*, vol. 55, n 2, April 2019.
- [19] Nguyen-Hong N, Nguyen-Duc H, Nakanishi Y. "Optimal sizing of energy storage devices in isolated wind-diesel systems considering load growth uncertainty," *IEEE Transactions on Industry Applications*. Vol. 54, no 3, pp 1983-91, May 2018.
- [20] A. Dolara, R. Faranda, and S. Leva, "Energy comparison of seven MPPT techniques for PV systems," *Journal of Electromagnetic Analysis and Applications*, vol. 1, no. 03, p. 152, Sept. 2009.
- [21] J. Xu, C. Lott, S. Saadate, and B. Davat, "Simulation and experimentation of a voltage source active filter compensating current harmonics and power factor," in *Proceeding of IECON'94-20th Annual Conference of IEEE Industrial Electronics*, 1994, vol. 1, pp. 411-415.



Félix Dubuisson (S'18) received the M.Sc. degrees in electrical engineering from the École de Technologie Supérieure Montreal, QC, Canada, where he is currently working toward Ph.D. degree. He is currently studying the predictive control for an off-grid system using renewable energy sources. His research interests include control and

design of microgrids, renewable energy generations and applications, and energy storage systems.



Miloud Rezakallah (S'11–M'14) received the B. Tech. degree in electrical machines and drive from the University of Science and Technology USTO, Oran, Algeria, and the M. Tech. and Ph.D. degrees in power electronics and system control from École de Technologie Supérieure, Université, Montréal, Canada., in 2010 and 2016, respectively. He is working as researcher at research center on smart grids and energy systems (Inergia Lab) at spet-iles in Quebec and as a research assistant in Electrical Engineering Department at École de Technologie Supérieure and his research interests include control and design of microgrid, power quality, renewable energy generations and applications, power management in smart grid, and energy storage systems.



Ambrish Chandra (SM'99–F'14) is a full professor of Electrical Engineering at École de technologie supérieure (ÉTS), Montréal since 1999. He received B.E. degree from the University of Roorkee (presently IITR), India, M. Tech. from IIT Delhi, and Ph.D. from University of Calgary, in 1977, 1980, and 1987, respectively. Before joining as an Associate Professor at ÉTS in 1994, he worked as a faculty at IITR. From 2012-15, he was the director of multidisciplinary graduate program on Renewable Energy and Energy Efficiency at ÉTS. The primary focus of his work is related to the advancement of new theory & control algorithms for power electronic converters for power quality improvement in distribution systems & integration of renewable energy sources. He is coauthor of John Wiley book 'Power Quality – Problems and Mitigation Techniques'. He is Fellow of many organizations, including Canadian Academy of Engineering, Institute of Engineering and Technology U.K., Engineering Institute of Canada etc. and registered as a Professional Engineer in Quebec. He is a Distinguished Lecturer of the IEEE Power and Energy Society and the IEEE Industry Application Society. He is the recipient of IEEE Canada 'P. Ziogas Electric Power Award 2018'.



Maarouf Saad received a bachelor and master degrees in electrical engineering from Ecole Polytechnique de Montreal respectively in 1982 and 1984. In 1988, he received a Ph.D. from McGill University in electrical engineering. He joined Ecole de technologie supérieure in 1987 where he is teaching control theory. His research

is mainly in nonlinear control and optimization applied to robotics and power systems.



Marco Tremblay is the R&D Director at Suez Water Technologies & Solutions in Montreal, Canada, developing industrial power electronic and control products. He is a licensed professional engineer with a bachelor degree from McGill University. He later obtained a Master degree from École de Technologie

Supérieure de Montréal where he is presently a PhD candidate. His major contribution has been the development of innovative products used to purify drinking water for more than fifty million people around the world and to reduction industrial pollution. He is presently studying the use of neural networks in equipment condition monitoring and diagnostics.



Hussein Ibrahim received the PhD degree in engineering from Québec University at Chicoutimi, Canada. Since July 2009, he has research director at Cégep of Sept-îles in the north of Quebec. His research interests include renewable energy sources integration, hybrid energy power system, storage energy, heat and mass transfer, fluid dynamics, and energy efficiency.